Path Planning for gliders using Regional Ocean Models: Application of *Pinzón* path planner with the ESEOAT model and the RU27 trans-Atlantic flight data

Enrique Fernández-Perdomo*, Jorge Cabrera-Gámez*, Daniel Hernández-Sosa*,
Josep Isern-González*, Antonio C. Domínguez-Brito*,
Alex Redondo†, Josep Coca†, Antonio G. Ramos†,
Enrique Álvarez Fanjul‡ and Marcos García‡
*University Institute of Sistemas Inteligentes y Aplicaciones Numéricas en Ingeniería (SIANI)
Universidad de Las Palmas de Gran Canaria, Las Palmas de Gran Canaria, Spain
{ efernandez, jcabrera, dhernandez, jisern, adominguez } @ iusiani.ulpgc.es
†Department of Biology
Universidad de Las Palmas de Gran Canaria, Las Palmas de Gran Canaria, Spain
{ aredondo, jcoca, aramos } @ pesca.gi.ulpgc.es
‡Puertos del Estado
Ministerio de Fomento (Gobierno de España), Madrid, Spain
{ enrique, marcos } @ puertos.es

Abstract— **Unmanned Underwater Vehicles (UUVs) are commonly used in Oceanography due to their relative low cost and wide range of capabilities. Gliders, being UUVs, are particularly suitable for long-range missions because of their large autonomy. They change their buoyancy to dive and climb describing a vertical saw tooth route, which produces an effective but low horizontal speed. This makes them strongly sensitive to ocean currents, and therefore, they might have to adapt the heading to the current field.**

In this article we outline a new path planning software named *Pinzón* to assist UUVs piloting, that integrates a novel path planning algorithm called CTS-A* (Constant-Time Surfacing A*). It manages ocean currents provided by Regional Ocean Models (ROMs) that capture their high temporal variability, which affects the vehicle trajectory significantly. This kind of path planning tools are particularly useful for gliders, especially for long-range missions.

In this work, we consider a particular region traveled by the RU27 *"Scarlet Knight"* glider in the trans-Atlantic mission. We focus on the last weeks of the mission, when the glider crossed the Spanish EEZ, from $14°$W to $12°$W meridian. It is possible to compare the path planner output to that of a direct path to the goal, or even the RU27 path. We have used a ROM provided by the ESEOO project for the Spanish Atlantic shore, known as ESEOAT. It provides ocean currents hourly, which capture the high variability of the currents in the zone. For this reason, daily means or other ocean models are generally unsuitable.

I. Introduction

Gliders are a new technology in active development, which has proven very promising in Ocean Research, and it is meant to be an important observational tool in the coming years [1]. Due to their low surge speed, gliders are far more affected by ocean currents than other UUVs that can overcome them. Contrary, gliders might drift significantly from its planned trajectory, making path planning a crucial tool. The importance of path planning for glider navigation lies precisely in this fact.

There exists a number of path planning techniques that comprises Linear Programming [2], [3], Potential fields [4], probabilistic sampling methods like Rapidly-Exploring Random Trees (RRTs) or Genetic Algorithms (GAs) [5], and Artificial Intelligence (AI) methods like A*, that assures the path optimality [6], [7], [8]. Several authors have applied some of these methods to the scope and singularities of glider navigation using ROMs [9], [10], [11], [12], [13]. Unfortunately, some AI techniques are not applicable to this context in principle. Some examples are the Theta* algorithm [14] that demands the existence of obstacles in the environment, which is not the case, and incremental methods such as D* Lite [15] and Incremental Phi* [16], that are thought to deal with relatively small changes in the environment, but not with highly time-varying ocean currents.

Path planning algorithms require a vehicle motion model to perform a correct trajectory estimation. Elaborated glider motion models have been discussed thoroughly in several works [17], [18]. The glider kinematics or dynamics might catch different factors that could affect the glider trajectory significantly. However, for long-range path planning it suffices

978-1-4244-5222-4/10/$26.00 ©2010 IEEE

with simplified models.

In this paper, we propose a path planning algorithm that incorporates ocean currents and a glider model affected by them. We can exploit both the temporal dynamics of ocean currents, as well as their 3D variability. To find the optimal path we start from an A* algorithm [7], which is modified and adapted to the problem specificities. Recall that standard A* discretizes the search space with an uniform grid, so the possible bearings are discretized too. Besides, this algorithm is usually applied in Robotics to find the path of lowest cost in static environments with obstacles. Some authors [9], [10], [11], [19], [13] have applied this AI path planning method for gliders moving through an uniform grid of ocean currents. The time between consecutive surfacings is non-constant then.

Instead of finding the path over an uniform grid, that would produce unrealistic non-constant time surfacings, we have engineered the path finder to obtain constant time surfacings. We allow any bearing angle and integrate the actual glider trajectory, which is strongly conditioned by the currents.

Our approach manages continuous space and time domains, which is reflected in the glider trajectory integration, that considers the effect of currents. Since the glider is no longer forced to reach a node of a grid, any bearing is allowed. The drift effect produced by ocean currents gives more precise trajectories, and the bearings obtained are more realistic and informed thus. Gliders might be commanded a new bearing when they surface. In fact, RU27 was programmed to surface periodically every $8\mathrm{h}$ for this purpose. This mode of operation has inspired our proposal. Furthermore, different goal specifications might be given, e.g. exact location, circular area, meridian-based, and it is possible to avoid forbidden areas.

We begin by describing our path planning approach based upon A* in Sec. II. The essential aspects are detailed and compared with the classical A* algorithm. Sec. III discusses Ocean Models that provide ocean currents among other data. The discussion is particularized in ROMs and a synthetic current field generator developed to control some features of the resulting ocean currents. Finally, some tests of the path planner on different scenarios are shown.

II. *Pinzón* PATH PLANNER

The path planning method discussed in this paper builds upon A* [7], shown in Alg. 1. To focus its search, A* uses h-values $h(n)$ that approximate the goal distances of the nodes $n \in \mathcal{N}$ using an heuristic function. In the special case where $h(n) = 0\ \forall n$ we have Dijkstra's algorithm [20], which main drawback is the fact that it does a blind search. Therefore, the ultimate purpose of the heuristic is to reduce the computational cost of the search.

The algorithm minimizes the distance to the goal, which in our case consists on a temporal cost based on the maximum speed a glider can achieve within the ocean current field and the great circle distance between a pair of locations $\mathbf{x}_i$ and $\mathbf{x}_j$ for $i \neq j$. The great circle distance is the shortest distance on a sphere or ellipsoid that in this case approximates the Earth surface, but a simpler metric distance might be used.

A* maintains for every node n:

1) The g-value $g(n)$, that is the distance of the shortest path from the start node n_{start} to the node n found so far.
2) The parent node of n, which is used to retrieve the path after the search ends. For the problem on hand, the path consists on a sequence of bearing angles θ_g that are to be commanded to the glider, and the computed surfacing locations $\mathbf{x}$.

It also maintains two global data structures:

1) The open list $\mathcal{O}$, which consists on a priority queue that contains nodes to be considered for expansion, along with the expected cost $f(n) = g(n) + h(n)$ to reach the goal n_{goal}.
2) The closed list $\mathcal{C}$, which contains nodes that have already been expanded in order to ensure that each node is expanded only once.

Algorithm 1 A*

Require: Start n_{start} and goal n_{goal} nodes.
Ensure: Optimal path $\mathcal{P}$ found from n_{start} to n_{goal}.
Algorithm: A*(n_{start}, n_{goal}) **return** $\mathcal{P}$

$g(n_{\text{start}}) = 0$
parent$(n_{\text{start}}) = n_{\text{start}}$ ▷ might assign null pointer $\varnothing$ too
$\mathcal{O} = \mathcal{C} = \varnothing$ ▷ empty open and closed lists
$\mathcal{O}$.**insert**$(n_{\text{start}}, g(n_{\text{start}}) + h(n_{\text{start}}))$
while $\mathcal{O} \neq \varnothing$ **do**
    $n_i = \mathcal{O}$.**pop** ▷ retrieve node n_i with lowest cost
    if $n_i = n_{\text{goal}}$ **then** ▷ goal n_{goal} reached
        return $\mathcal{P}$ ▷ path found (extracted from parent$(\cdot)$)
    end if
    $\mathcal{C} = \mathcal{C} \cup \{n\}$
    for all $n_{i+1} \in$ **successors**(n_i) **do**
        if $n_{i+1} \notin \mathcal{C}$ **then**
            if $n_{i+1} \notin \mathcal{O}$ **then**
                $g(n_{i+1}) = \infty$
                parent$(n_{i+1}) = \varnothing$
            end if
            if $g(n_i) + c(n_i, n_{i+1}) < g(n_{i+1})$ **then**
                $g(n_{i+1}) = g(n_i) + c(n_i, n_{i+1})$ ▷ update
                parent$(n_{i+1}) = n_i$
                if $n_{i+1} \in \mathcal{O}$ **then**
                    $\mathcal{O}$.**remove**(n_{i+1})
                end if
                $\mathcal{O}$.**insert**$(n_{i+1}, g(n_{i+1}) + h(n_{i+1}))$
            end if
        end if
    end for
end while
return $\varnothing$ ▷ no path found

A* updates the g-value and parent of an unexpanded successor n_{i+1} of node n_i by considering the distance $g(n_i)$ of the path from n_{start} and the distance $c(n_i, n_{i+1})$ from n_i to n_{i+1}, resulting in $g(n_i) + c(n_i, n_{i+1})$. It updates the g-value and parent of n_{i+1} if the new path distance $g(n_{i+1})$ is shorter than the shortest path from n_{start} to n_{i+1} found so far (see line 18 of Alg. 1).

In general, there are not obstacles in the sea, but ocean currents might not permit the vehicle to move in a particular direction. This is a slightly different problem than the original one for which A* was designed. In the original A* algorithm, the **successors** procedure generates the list of neighbors n_{i+1} of the current node n_i assuming an 8-neighborhood in an uniform grid. Contrary, our Constant-Time Surfacing A* (CTS-A*) operates radically different.

Our approach includes a notable modification to the original A* algorithm. As a consequence of forcing constant time surfacings, the process of generating successors changes:

1) For each bearing θ_{g_j} we integrate the glider trajectory for the surfacing time t_s, i.e. we compute the trajectory followed by a glider that keeps a bearing θ_{g_j} under the influence of instantaneous ocean currents.
2) The final location of each trajectory is stored in the Nearest Neighbor node $n_{i+1}^{\theta_{g_j}}$ of a grid. Special care is taken to avoid overwriting, which requires the successors generation procedure to be hard-coded alongside the open list $\mathcal{O}$ update step.
3) If two locations fall into the same node, we take the one with lower cost. If both have the same cost, we take the closest to the node.

The major change is centered on the generation of successors. This modification is concerned with the node labeling and the closed list $\mathcal{C}$ management. Alg. 2 sums up the generation of successors process for clarity.

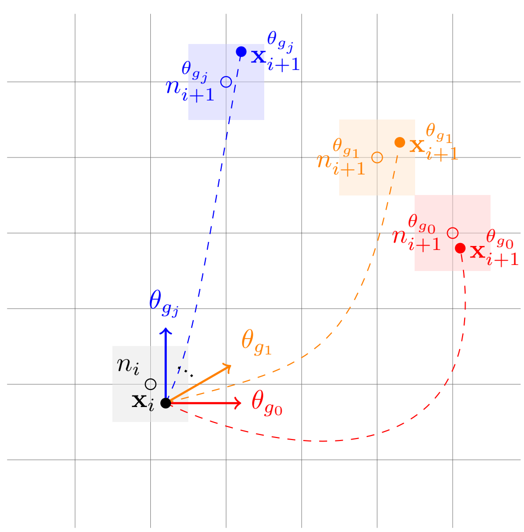

Fig. 1

SUCCESSORS GENERATION IN THE CTS-A* APPROACH PROPOSED. STARTING AT A NODE n_i SEVERAL TRAJECTORIES ARE INTEGRATED FOR SURFACING TIME t_s CONSIDERING DIFFERENT BEARINGS θ_{g_i} STARTING FROM LOCATION $\mathbf{x}_i$

The path finding basis of our approach is depicted in Fig. 1. For each surfacing location $\mathbf{x}_i$, starting with $n_{\text{start}} = n_0$, the

Algorithm 2 Successors generation in CTS-A*

Require: Current node n, the number k of bearings to sample and the surfacing time t_s to integrate the trajectory. The trajectory integration requires the integration step dt, the glider nominal speed $\mathbf{v}_g(\theta_g)$ for a bearing θ_g, and the current field $\mathbf{v}_c(\mathbf{x})$.

Ensure: Successors list $\mathcal{N}$ and node labeling update considering the cost $c(\mathbf{x})$ and the distance $d(\mathbf{x}, m)$ of the location $\mathbf{x}$ paired with the node m.

Algorithm: **successors**(n, k, t_s) **return** $\mathcal{N}$

1: $\mathcal{N} = \varnothing$
2: **for all** 1 to k **do**
3: $\quad \theta_g \sim [0, 2\pi)$ ▷ sample bearing
4: $\quad \mathbf{x}_{\theta_g} =$ **trajectory**$(t_s, dt, \mathbf{v}_g(\theta_g), \mathbf{v}_c(\mathbf{x}), \mathbf{x}_n)$
5: $\quad m =$ **NN**$(\mathbf{x})$ ▷ Nearest Neighbor node m to $\mathbf{x}$
6: $\quad$ **if** $m \notin \mathcal{C}$ **then** ▷ m cannot be in the closed list $\mathcal{C}$
7: $\quad\quad$ **if** m already labelled **then** ▷ labelled with $\mathbf{x}_m$
8: $\quad\quad\quad$ **if** $c(\mathbf{x}_{\theta_g}) < c(\mathbf{x}_m)$ **then** ▷ lower cost
9: $\quad\quad\quad\quad$ label m with $\mathbf{x}_{\theta_g}$
10: $\quad\quad\quad$ **else if** $c(\mathbf{x}_{\theta_g}) = c(\mathbf{x}_m)$ **then** ▷ equal cost, but
11: $\quad\quad\quad\quad$ **if** $d(\mathbf{x}_{\theta_g}, m) < d(\mathbf{x}_m, m)$ **then** ▷ closer
12: $\quad\quad\quad\quad\quad$ label m with $\mathbf{x}_{\theta_g}$
13: $\quad\quad\quad\quad$ **end if**
14: $\quad\quad\quad$ **end if**
15: $\quad\quad$ **else**
16: $\quad\quad\quad$ label m with $\mathbf{x}_{\theta_g}$
17: $\quad\quad$ **end if**
18: $\quad\quad \mathcal{N} = \mathcal{N} \cup \{m\}$ ▷ add m to successors list $\mathcal{N}$
19: $\quad$ **end if**
20: **end for**
21: **return** $\mathcal{N}$

glider trajectory is integrated for the surfacing time t_s for different bearing angles θ_{g_j}. This process is repeated with the new surfacing locations generated, $\mathbf{x}_{i+1}^{\theta_{g_0}}$, $\mathbf{x}_{i+1}^{\theta_{g_1}}$ and $\mathbf{x}_{i+1}^{\theta_{g_j}}$ in the figure, which are selected according to the cost function that guides the searching to the goal node n_{goal}. The locations $\mathbf{x}_{i+1}^{\theta_{g_j}}$ are not discretized, since they are saved in the Nearest Neighbor node $n_{i+1}^{\theta_{g_j}}$ of a grid that discretizes the search space.

As a consequence of using a temporal cost with a constant surfacing time t_s, the following relations holds

$$c(\mathbf{x}_{\theta_g}) = c(\mathbf{x}_n) + t_s \qquad (1)$$

where $\mathbf{x}_n$ is the current node location, $\mathbf{x}_{\theta_g}$ is the successor node location taking the bearing θ_g for a surfacing time t_s. Therefore, all successors of a particular node n have the same cost, simplifying the implementation.

Ideally, all bearing angles would be considered for trajectory integration. Unfortunately, it is computationally expensive to test so many bearings, and therefore we must take a subset of samples intelligently. The sampling process to obtain k bearings, that takes place in line 3 of Alg. 2, can be uniformly distributed or it might follow a PDF (Probability Density Function) distribution.

A. Glider motion model

Given the ocean current field and a glider kinematic or dynamic model, it is possible to simulate the actual trajectory described by the vehicle. However, both the ocean model that computes the current field and the glider model are uncertain. There exists a number of works that model glider dynamics [18], [17], but in general, the glider kinematics suffices to model the vehicle motion for long-range missions.

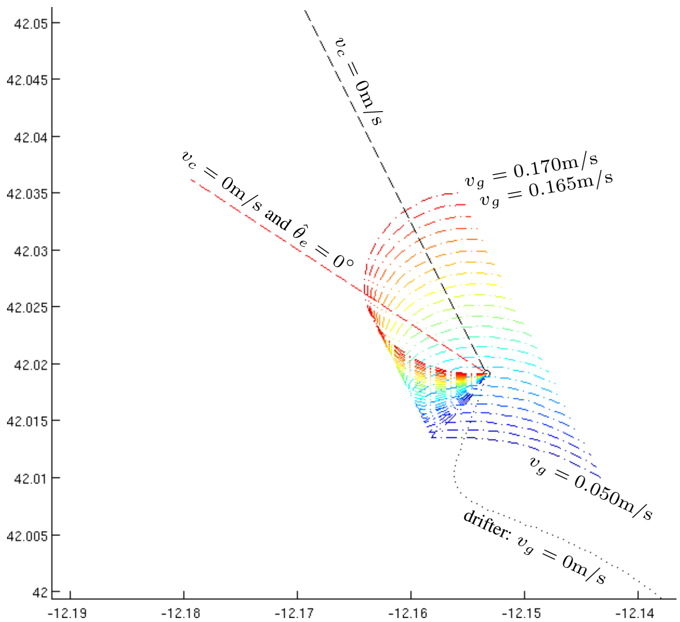

Fig. 2

TRAJECTORIES DESCRIBED BY THE GLIDER CONSIDERING A CONSTANT HEADING ERROR OF $\hat{\theta}_e = 30°$N FOR DIFFERENT GLIDER SPEEDS v_g

In the present work, we consider a glider kinematic model and the effect of different phenomena. Probably, the heading error $\hat{\theta}_e$ and the glider nominal speed v_g are the most remarkable factors, since they degrade systematically throughout the mission due to biofouling, as could be observed during the final part of RU27 flight. The heading error $\hat{\theta}_e$ is a measure of the deviation from the heading due to the drift correction shown in Fig. 5, probably induced by several coupled, nonlinear or unpredictable factors. Both $\hat{\theta}_e$ and v_g have a high impact in the resulting trajectory followed by the glider, as shown in Fig. 2 and 3. For instance, there exists a strong influence of the current field over time and a tight dependence on the heading error that might be affecting the glider dynamics. The resulting trajectories are also affected by the glider nominal speed, since it determines whether the glider can beat the current. However, comparing Fig. 2 and Fig. 3, we observe that the effect of the heading error is clearly more significant. Thus, if $\hat{\theta}_e$ were known, it will be possible to estimate the actual glider speed v_g using the surfacing locations $\mathbf{x}_i$, as shown in Fig. 4. Mostly, these factors have been estimated using the data retrieved by the RU27 glider in

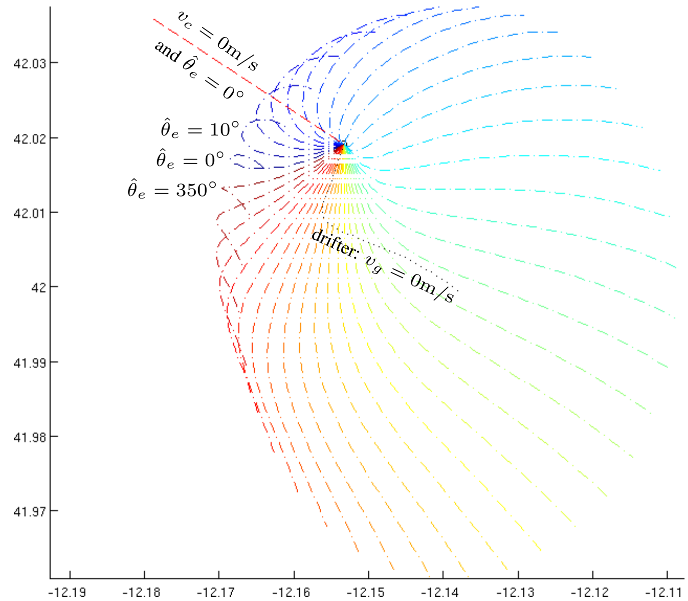

Fig. 3

TRAJECTORIES DESCRIBED BY THE GLIDER CONSIDERING A CONSTANT GLIDER SPEED OF $v_g = 15\mathrm{cm/s}$ FOR DIFFERENT HEADING ERROR ANGLES $\hat{\theta}_e$

the trans-Atlantic mission headed by Rutgers University.

It is possible to adapt A* to the problem at hand using a kinematic motion model constrained by the drift correction need to beat the ocean currents basically. Given the glider nominal speed v_g, the desired course or heading θ_e, and the ocean current speed v_c and direction θ_c, we can compute the drift correction that the glider must apply to keep such heading. Thus, we obtain the bearing θ_g

$$\theta_g = \begin{cases} \theta_e + \arcsin s & \text{if } |s| \leq 1 \\ \nexists & \text{otherwise} \end{cases} \tag{2}$$

and the resulting speed v_e

$$v_e = \begin{cases} v_g\sqrt{1-s^2} + v_c \cos\theta_{ec} & \text{if } |s| \leq 1 \\ 0 & \text{otherwise} \end{cases} \tag{3}$$

where

$$s = \frac{v_c}{v_g} \sin\theta_{ec} \tag{4}$$

and $\theta_{ec} = \theta_e - \theta_c$.

In Fig. 5 is depicted the vector composition of the drift correction process. Notice that all this velocities $v_\cdot$ are not vectors, but magnitudes $\|\mathbf{v}_\cdot\|$. We assume $v_e = 0$ when it is not possible to keep a particular heading θ_e. This is usually a consequence of a low glider speed v_g relative to the ocean current speed v_c, which forces the glider to navigate following the ocean current direction θ_c.

As a consequence of the important effect of the spatial and temporal variability of ocean currents, we do not constrain the glider heading θ_e to those angles that can actually be kept

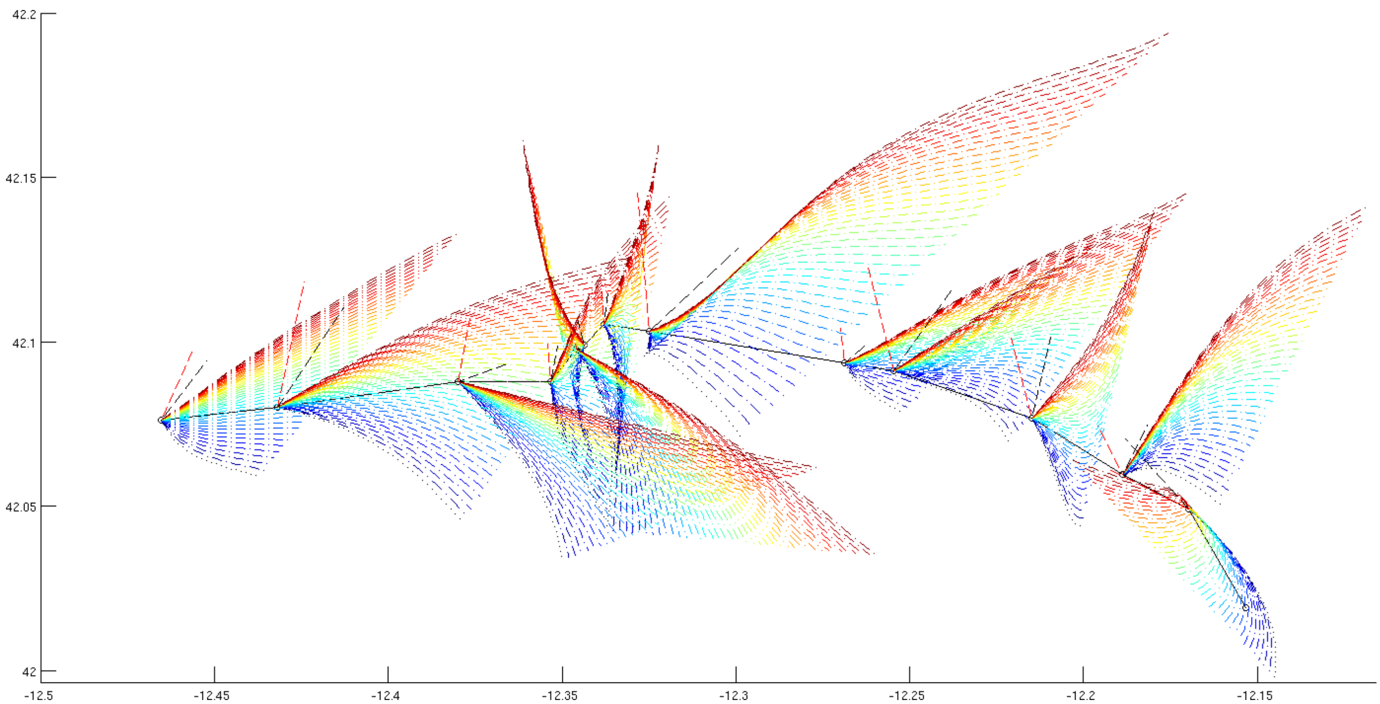

Fig. 4

SERIES OF TRAJECTORIES VARYING v_g FROM $0.01\mathrm{m/s}$ -·-·- TO $0.40\mathrm{m/s}$ -·-·- WITH $0.01\mathrm{m/s}$ INCREMENTS. GIVEN THE HEADING ERROR $\hat{\theta}_{e_i}$ WE MAY ANALYZE THE EFFECT OF v_g FOR DIFFERENT SURFACING LOCATIONS OF THE RU27 PATH (GROUND TRUTH) $\mathbf{x}_i$ ——. THE TRAJECTORIES FOR $v_c = 0\mathrm{m/s}$ - - - , $v_c = 0\mathrm{m/s}$ AND $\hat{\theta}_e = 0°$ - - - , AND A DRIFTER ($v_g = 0\mathrm{m/s}$) ······ ARE SHOWN TOO.

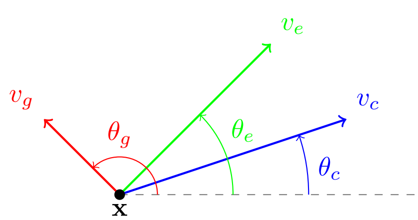

Fig. 5

VECTOR COMPOSITION FOR DRIFT CORRECTION. A BEARING θ_g MUST BE COMMANDED TO OBTAIN A HEADING OR COURSE θ_e THAT CAN BEAT A CURRENT OF DIRECTION θ_c. THE RESULTING EFFECTIVE VELOCITY v_e DEPENDS ON THE GLIDER SPEED v_g AND THE CURRENT SPEED v_c

according to (3) —in some cases this will lead to very few heading angles. Contrary, we use an unconstrained kinematic motion model where the resulting effective speed $\mathbf{v}_e$ is given by

$$\mathbf{v}_e = \mathbf{v}_g + \mathbf{v}_c \tag{5}$$

where $\mathbf{v}_g$ is the glider nominal speed and $\mathbf{v}_c$ is the speed of the ocean current through the path $\mathcal{P}$ described by the glider. Since $\mathbf{v}_c$ is different at each point in the environment, we must integrate the velocity through $\mathcal{P}$. Hence,

$$\mathbf{v}_e = \mathbf{v}_g + \int_{\mathbf{x}_{i-1}}^{\mathbf{x}_i} \mathbf{v}_c(\mathbf{x})\, d\mathbf{x} \tag{6}$$

for $\mathcal{P}$ starting at $\mathbf{x}_{i-1}$ and ending at $\mathbf{x}_i$ locations, that will correspond to surfacing points.

The integration is typically discretized and performed for a fixed surfacing time t_s. Such integration allows to obtain the glider trajectory under the current field conditions. The integration algorithm is summarized in Alg. 3.

Algorithm 3 Trajectory integration

Require: Surfacing time t_s and integration step dt. Glider nominal speed $\mathbf{v}_g$, current field $\mathbf{v}_c(\mathbf{x})$ for all locations $\mathbf{x}$, and initial location $\mathbf{x}_0$.

Ensure: Final location $\mathbf{x}$ after integrating the trajectory for t_s time.

Algorithm: **trajectory**(t_s, dt, $\mathbf{v}_g$, $\mathbf{v}_c(\mathbf{x})$, $\mathbf{x}_0$) **return** $\mathbf{x}$

1: $\mathbf{x} = \mathbf{x}_0$ ▷ Initial location
2: **for all** $t = 0$ to t_s with step dt **do**
3: $\mathbf{v}_e = \mathbf{v}_g + \mathbf{v}_c(\mathbf{x})$
4: $\mathbf{x} = \mathbf{x} + \mathbf{v}_e \cdot dt$
5: **end for**
6: **return** $\mathbf{x}$

When computing the heuristic, we need an estimate of the maximum velocity $v_{c_{\max}} = \max_{\mathbf{x} \in \mathcal{P}}(\|\mathbf{v}_c(\mathbf{x})\|)$ of the ocean currents through the final path $\mathcal{P}$ that the glider will follow. Since $\mathcal{P}$ is unknown in advance, we estimate this maximum velocity considering the ocean current field of the whole domain Ω provided by the ROM. Given $v_{c_{\max}}$ we can compute an underestimated temporal cost to reach the goal from the current location $\mathbf{x}_i$, using the straight distance $d = \|\mathbf{x}_i - \mathbf{x}_{\text{goal}}\|$ to the goal,

$$h(\mathbf{x}) = t = \frac{d}{v_g + v_{c_{\max}}} \tag{7}$$

which is the heuristic function, having a temporal meaning.

III. Ocean Model

In the present work, we have fed our path planner with a Regional Ocean Model (ROM) because we have focused in the last stings of the RU27 trans-Atlantic mission, when the glider traveled the Spanish EEZ. We use a ROM developed by Puertos del Estado (Ministerio de Fomento, Gobierno de España) as part of the project ESEOO, that covers the Spanish Atlantic shore. It provides temporal series hourly with 3-day predictions at $0.05°$ spatial resolution. The ROM output is validated with samples taken *in situ* by oceanographic sensor networks. Thus, the ROM is meant to provide accurate data, capturing the high temporal dynamics of the area, especially during the RU27 journey.

Although the ROM provides several data, it is possible to plan paths using ocean currents only, because they are not geostrophic currents simply. Anyway, additional physical parameters might be incorporated easily.

Additionally, we have developed a synthetic current field generator based on [19] to assist the production of controlled test cases —e.g. current strength, eddies size. It generates a synthetic current field from a streamfunction $\Psi(\mathbf{x})$, that resembles the Sea Surface Height Anomaly (SSHA).

IV. Results

In order to compare the results obtained, apart from our Constant-Time Surfacing A* approach, we consider a naive Direct-to-Goal (DtG) strategy and a classical A* adapted to manage ocean currents and the constrained motion model of (2), (3) and (4). Figures 6, 7 and 8 illustrate the different mode of operation of these three approaches, respectively. The DtG approach is equivalent to the way the RU27 glider was piloted, except for the fact that the goal waypoint was used to set its bearing θ_g.

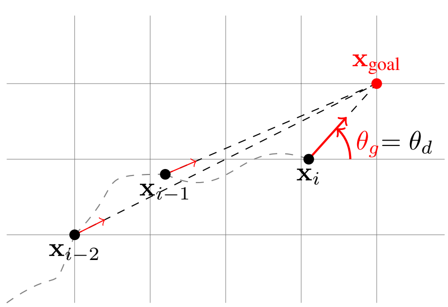

Fig. 6
Direct-to-Goal approach, that sets a bearing θ_g equal to the heading θ_d to the goal $\mathbf{x}_{\text{GOAL}}$ from the current location $\mathbf{x}_i$

While the DtG strategy sets the bearing $\theta_g = \theta_d$ in the straight direction to the goal, the other two methods explore several paths starting from the current location $\mathbf{x}_i$. In the case of A*, the algorithm establishes the cost of traveling from $\mathbf{x}_i$ to each of its neighbors, which imposes a set of heading angles θ_e. Due to ocean currents we will obtain non-constant time surfacings.

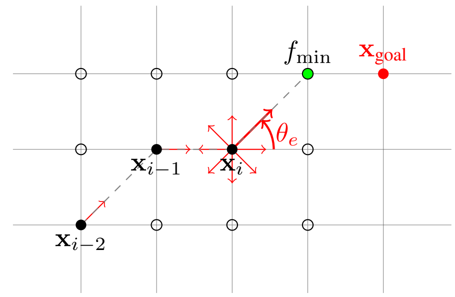

Fig. 7
Classical A* algorithm operating on an uniform grid that defines the search space domain Ω. The heading angles θ_e are constrained by the grid, producing straight line trajectories between nodes and non-constant surfacing times

Contrary, the CTS-A* considers a set of bearings θ_g to integrate the glider trajectory from $\mathbf{x}_i$ for the surfacing time t_s, generating constant-time surfacings. This procedure is closer to the way gliders operate, resulting in more realistic paths.

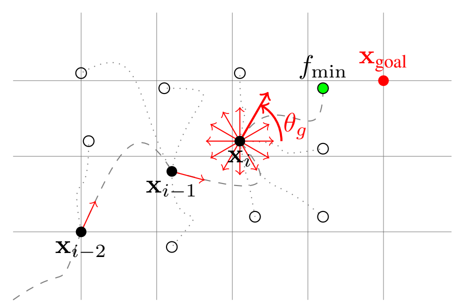

Fig. 8
Constant-Time Surfacing A* algorithm. At each surfacing location $\mathbf{x}_i$ different bearing angles θ_g are considered, integrating the glider trajectory for the surfacing time t_s

Apart from the results shown here, our *Pinzón* path planner is capable of outputting the resulting path in the form of a movie to illustrate the temporal dynamics of the current field and how the glider trajectory is affected. *Pinzón* also generates Google™ Earth animations in KML format (see Fig. 9), that allow to analyze the resulting path overlaid on the glider mission data, or even the weather.

Here, we illustrate the results that our CTS-A* approach produces on different scenarios. We consider the ocean current fields provided by the ESEOAT ROM introduced in Sec. III, for the period of time in which the RU27 glider crossed the

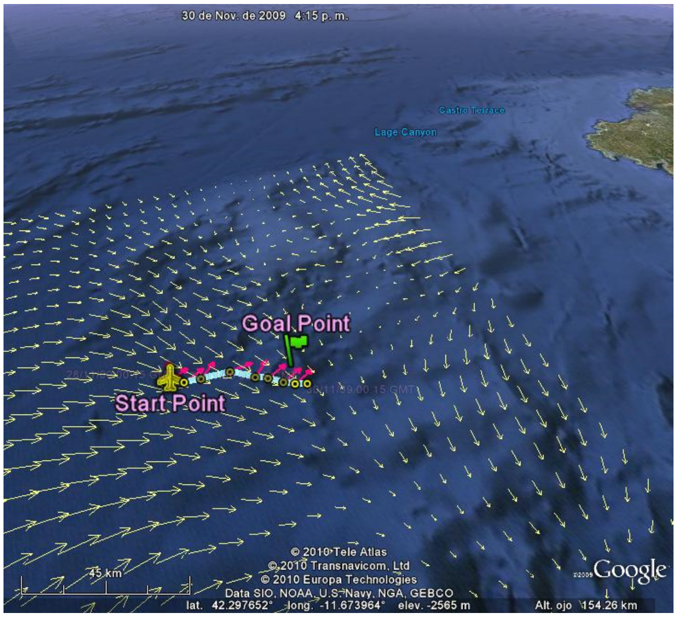

Fig. 9

EXAMPLE OF PATH PLANNED BY *Pinzón* USING THE ESEOAT ROM AND RU27 DATA TO ACHIEVE A MERIDIAN-BASED GOAL. THE OUTPUT IS A KML ANIMATION THAT CAN BE SHOWN IN GOOGLE™ EARTH

zone covered by this ROM. We try to analyze the performance under different conditions, such as the current strength and temporal variability. Additionally, the results are compared with the strategies mentioned above.

A. *CTS-A* comparison with other methods*

Fig. 10 depicts a typical path planning output. It shows the path found, which consists on a sequence of waypoint locations $\mathbf{x}_i$ and bearing angles θ_{g_i} that must be commanded to the glider. The bearing angles, along with the resulting heading angles θ_{e_i}, are shown as arrows emanating from each surfacing located at $\mathbf{x}_i$.

The glider trajectory due to the drift is drawn to illustrate the important effect of time-varying ocean currents. Bear in mind that the background ocean current field of Fig. 10 corresponds to the first time snapshot, because it is not possible to show it over time in a single frame. Thus, *Pinzón* produces movie clips to sort this issue out. Finally, the nodes visited or expanded by the algorithm are marked. This gives some insight on the searching process, that might be exhaustive or not depending on the problem on hand.

This output is the same for all the path planning methods discussed above. However, the comparison of Fig. 11 does not show the bearing angles θ_g among other additional information for clarity reasons. The RU27 path from the start node n_{start} is included too. We have considered the same glider nominal speed $v_g = 0.35\text{m/s}$ for each method, since the DtG approach does not find any path with slower values. This way, the

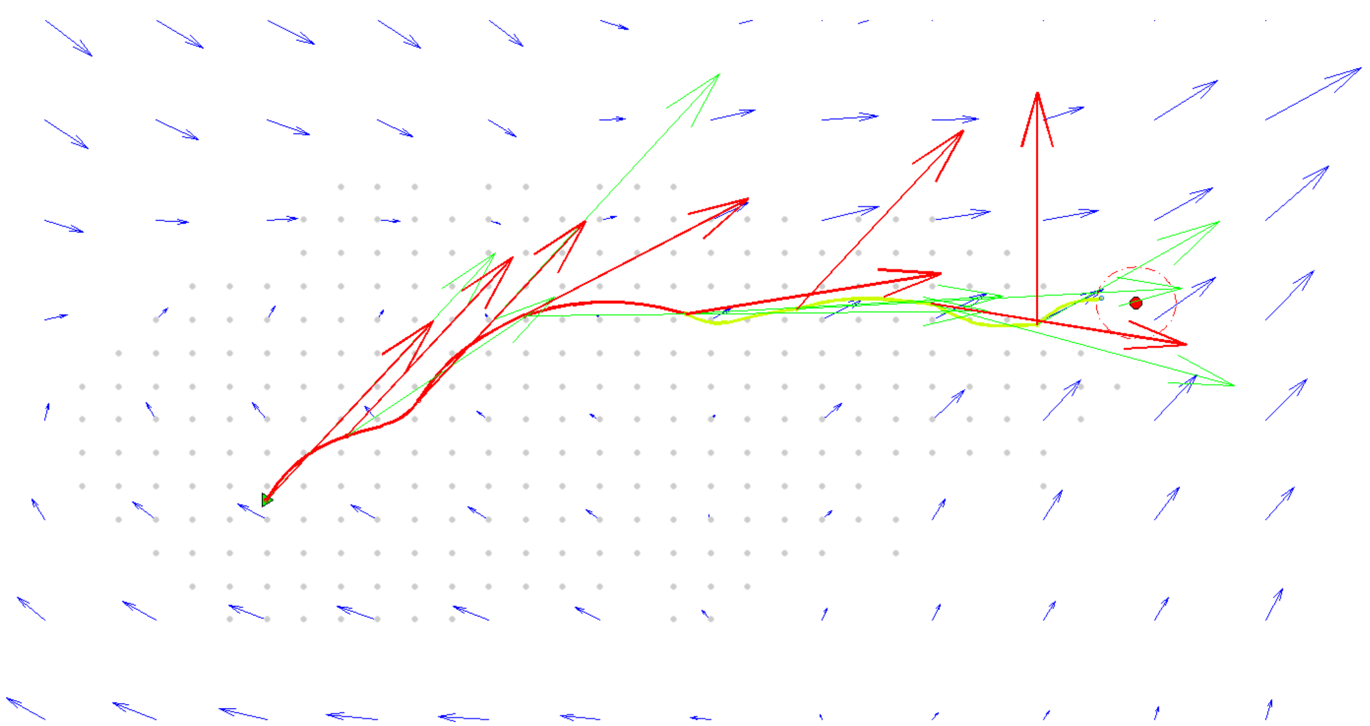

Fig. 10

CTS-A* OUTPUT SHOWS THE PATH PLANNED DRAWING THE GLIDER TRAJECTORY FROM THE START ▶ TO THE GOAL ● NODE. BACKGROUND BLUE ARROWS ⟶ SHOW THE CURRENT FIELD, WHILE **THICK RED** ⟶ AND GREEN ⟶ ARROWS ARE THE BEARING θ_g AND HEADING θ_e ANGLES

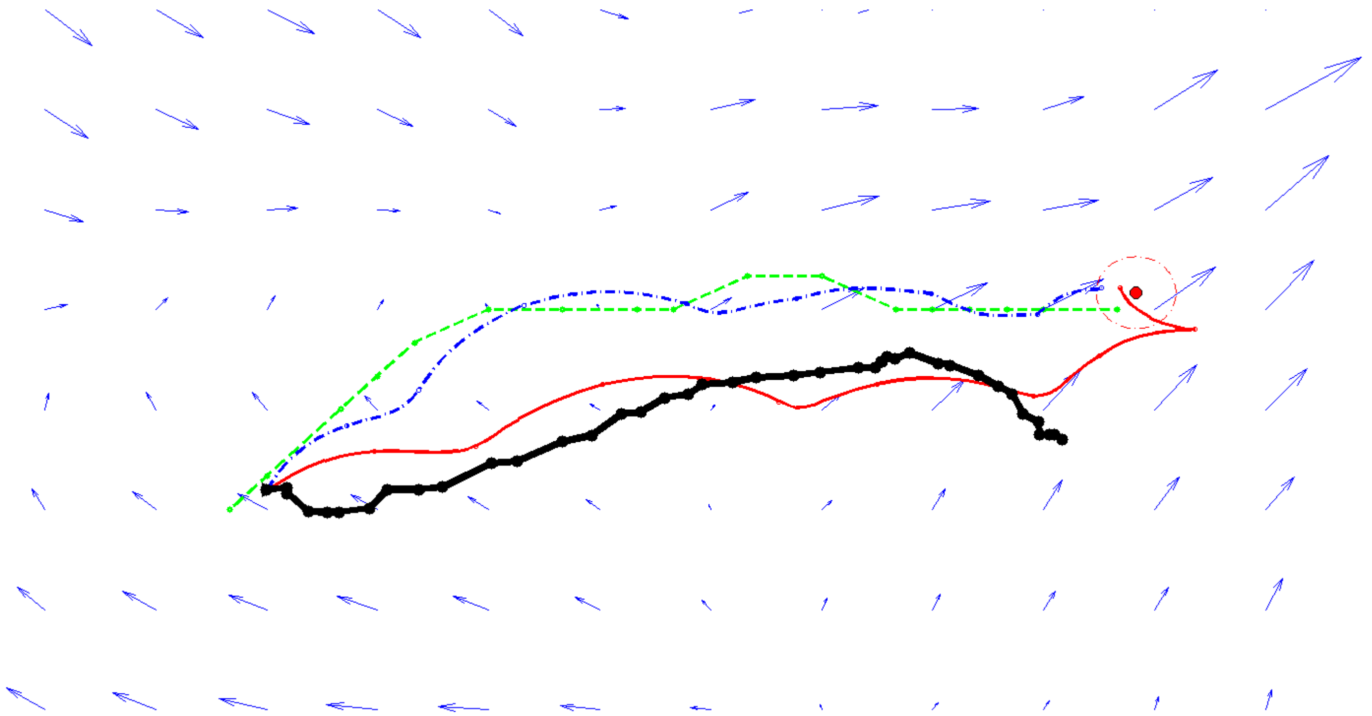

Fig. 11

COMPARISON OF PATHS PLANNED WITH DIFFERENT STRATEGIES FROM THE START NODE ▷ TO THE GOAL NODE ● FOR THE 21-NOV-2009: DTG ——, A* - - - AND CTS-A* -·-·-, ALONG WITH THE RU27 PATH ——

resulting paths are comparable then. Nevertheless, at this point of the mission the RU27 glider was traveling at a relatively slower nominal speed $v_g \approx 0.15\mathrm{m/s}$ as a consequence of the drag induced by biofouling. Hence, the RU27 path contains far more surfacings than the paths planned.

Both A* and CTS-A* find paths of lower cost than the DtG approach, that costs approximately $8\mathrm{h}$ more for this example. However, CTS-A* gives more realistic and informed results, since it integrates the glider trajectory through the time-varying ocean currents, regardless of the cost of the path, which might be higher or lower depending on the case.

B. Effect of the current field strength and eddies size

The effect of the current field strength actually relies on the speed ratio given by $\frac{v_{c_{\max}}}{v_g}$, that relates the glider nominal speed v_g and the maximum ocean current speed $v_{c_{\max}}$, used in (7). It determines if the glider can beat them. Interestingly, a nominal glider speed v_g increase is equivalent to navigate through weaker ocean currents.

For testing purposes we consider a given ocean current field and different values for v_g. Recall that the faster the nominal glider speed v_g, the smaller the aspect ratio, as shown in Fig. 12. For fast speeds (or weak ocean currents) the glider will be less sensitive to the drift, as observed in the more sinuous trajectory of the $v_g = 0.2\mathrm{m/s}$ case. Then, the resulting paths tend to the straight line from the start n_{start} to the goal n_{goal} nodes, as shown in Fig. 12. On the contrary, for slow speeds (or strong ocean currents) the path will follow the current field. Clearly, intelligent path planning is more important under strong ocean currents, or more specifically, when the speed ratio is high. In fact, for weak currents the DtG approach suffices to capture a nearly optimal path, and the trajectory integration of our CTS-A* algorithm becomes less influential and relevant.

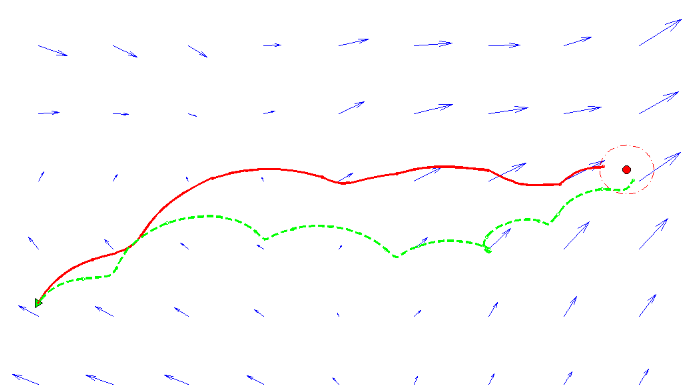

Fig. 12

PATHS PLANNED FOR THE 21-NOV-2009 CONSIDERING FAST $v_g = 0.35\mathrm{m/s}$ (SPEED RATIO OF 167.02%) —— AND SLOW $v_g = 0.2\mathrm{m/s}$ (SPEED RATIO OF 292.28%) - - - GLIDER NOMINAL SPEEDS, WHICH IS EQUIVALENT TO PATH PLANNING FOR WEAK AND STRONG CURRENTS, RESPECTIVELY

Similarly, it is possible to test the path planner for different

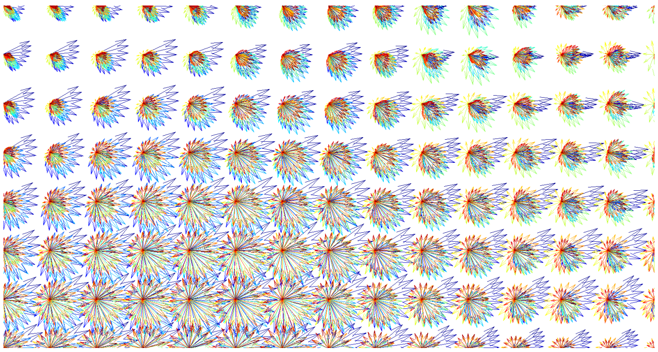

(a) Velocity field

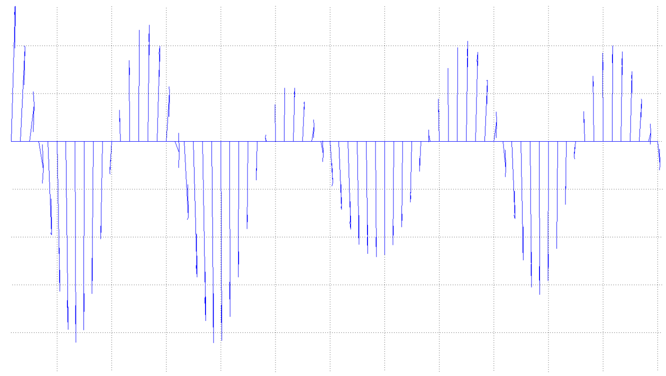

(b) Velocity plot

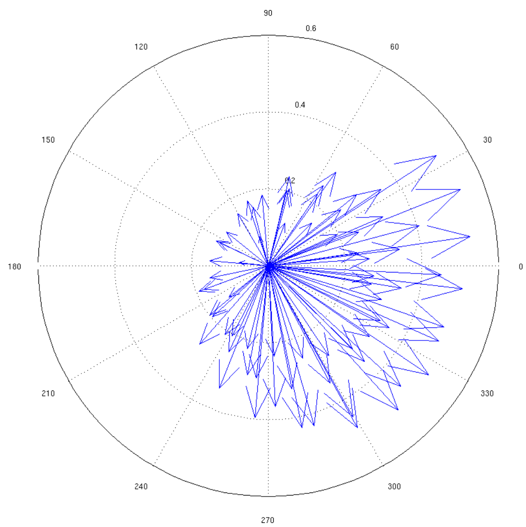

(c) Compass plot

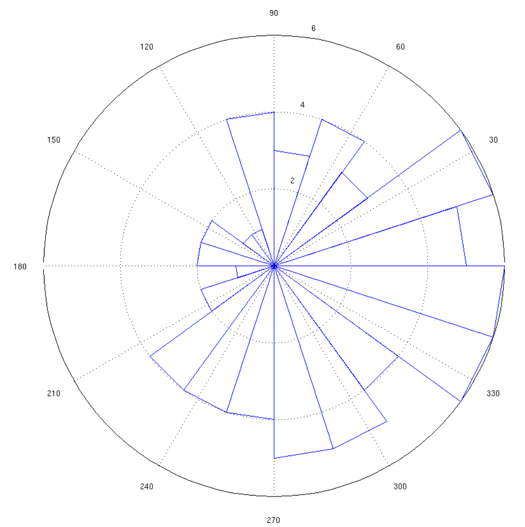

(d) Rose plot

Fig. 13

CURRENT TEMPORAL DYNAMICS IN THE ESEOAT ZONE FOR A WHOLE DAY, SHOWING (A) THE CURRENT FIELD AND (B)-(D) THE CURRENT SPEED AT A PARTICULAR LOCATION $\mathbf{x} = (42°\mathrm{N}, -13°\mathrm{E})$, USING HOURLY DATA FOR THE 21-NOV-2009

structures of the ocean currents. Eddies are common structures that may vary in size. When they are large, the resulting paths are more intricate, provided that the ocean currents are sufficiently strong. Therefore, path planning proves particularly useful in such cases, which where present in the area covered by the ESEOAT ROM. Indeed, during the RU27 flight eddies oscillated over time, as we will see in the sequel.

C. Effect of time-varying ocean currents

In Fig. 13 several plots illustrate the high temporal variability of ocean currents in the area covered by the ESEOAT ROM, which was crossed by the RU27 glider in its trans-Atlantic mission. Paths planned without considering the change of ocean currents over time will be less close to reality, not matter if they are more or less expensive.

Depending on the temporal variability in the study area, path planning over time will be more or less significant. Constant-time ocean currents are assumed to be daily means, instead of hourly series. Notice that for daily means, ocean currents are

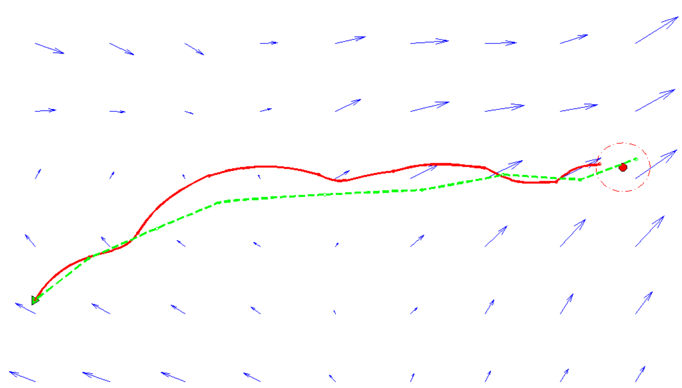

Fig. 14

PATHS PLANNED FOR TIME-VARYING —— AND CONSTANT (DAILY MEANS) - - - CURRENTS, USING THE ESEOAT ROM OCEAN CURRENTS FROM 21-NOV-2009 ONWARDS only interpolated for the last and first hour of two consecutive days. As Fig. 14 shows, time-varying currents yield glider trajectories that cannot be reproduced by simply using daily means. The zone covered by the ESEOAT ROM is precisely very time-varying, and it was under the influence of an inertial wave appreciable in Fig. 13 (b) when the RU27 glider flew it.

V. Conclusion

In this paper we introduce a Constant-Time Surfacing A* (CTS-A*) algorithm, a path planning method aimed to assist glider navigation that constitutes the core of a path planning software coined *Pinzón*. It uses time-varying 2D ocean current fields as provided by ROMs to integrate the glider trajectory over time. This approach ensures the optimality of the resulting path, which is an important feature of A* algorithms over other strategies like Genetic Algorithms or Linear Programming methods [2], [3], [4], [5]. Contrary to other approaches, like the naive Direct-to-Goal method and the classical A* algorithm, our CTS-A* method tries to generate more informed outputs, following the glider *modus operandi* faithfully.

In this work we have also discussed several factors that might establish the importance or need for intelligence path planning. Some of them are the eddies size, the ocean current strength, the glider nominal speed v_g and heading error θ_e.

VI. Further Work

Future research will be directed towards the application of our path planning approach to three dimensional ocean current fields. Since gliders describe a vertical saw tooth profile, the 3D dynamics are thought to affect the glider trajectory significantly. Indeed, it is known that ocean currents vary in depth describing a Ekman-like spiral.

In addition, we would study the use of a more elaborated motion model, being kinematic or dynamic, that incorporates additional factors in a physical correct manner.

Acknowledgement

This work is partially supported by the projects PI2007/039 funded by the Autonomous Government of Canary Islands (Gobierno de Canarias — Consejería de Educación, Cultura y Deportes, Spain) with FEDER funding, and TIN2008-06068 funded by the Ministerio de Ciencia e Investigación, Gobierno de España. The authors would like to thank Puertos del Estado for granting access to the ESEOAT ROM output, as well as Rutgers University for providing free access to the RU27 trans-Atlantic flight data.

References

[1] D. L. Rudnick, R. E. Davis, C. C. Eriksen, D. M. Fratantoni, and M. J. Perry, "Underwater Gliders for Ocean Research," *Marine Technology Society Journal*, vol. 38, no. 1, pp. 48–59, 2004.

[2] W. Zhang, T. Inanc, S. Ober-Blöbaum, and J. E. Marsden, "Optimal Trajectory Generation for a Glider in Time-Varying 2D Ocean Flows B-spline Model," in *IEEE International Conference on Robotics and Automation*, May 2008, pp. 1083–1088.

[3] N. K. Yilmaz, C. Evangelinos, P. F. J. Lermusiaux, and N. M. Patrikalakis, "Path Planning of Autonomous Underwater Vehicles for Adaptive Sampling Using Mixed Integer Linear Programming," *IEEE Journal of Oceanic Engineering*, vol. 33, no. 4, pp. 522–537, 2008.

[4] J. Witt and M. Dunbabin, "Go with the Flow: Optimal AUV Path Planning in Coastal Environments," in *Australasian Conference on Robotics and Automation (ACRA)*, 2008.

[5] D. Rao and S. B. Williams, "Large-scale path planning for Underwater Gliders in ocean currents," in *Australasian Conference on Robotics and Automation (ACRA)*, 2009.

[6] K. Walsh and B. Banerjee, "Fast A* with Iterative Resolution for Navigation," *International Journal on Artificial Intelligence Tools (IJAIT)*, vol. 19, no. 1, pp. 101–119, 2010.

[7] P. E. Hart, N. J. Nilsson, and B. Raphael, "A Formal Basis for the Heuristic Determination of Minimum Cost Paths," *IEEE Transactions on Systems Science and Cybernetics*, vol. 4, no. 2, pp. 100–107, Jul. 1968.

[8] K. P. Carroll, S. R. McClaran, E. L. Nelson, D. M. Barnett, D. K. Friesen, and G. N. William, "AUV path planning: an A* approach to path planning with consideration of variable vehicle speeds and multiple, overlapping, time-dependent exclusion zones," in *Proceedings of the 1992 Symposium on Autonomous Underwater Vehicle Technology (AUV'92)*, Jun. 1992, pp. 79–84.

[9] D. Wang, "Autonomous Underwater Vehicle (AUV) Path Planning and Adaptive On-board Routing for Adaptive Rapid Environmental Assessment," Ph.D. dissertation, Massachusetts Institute of Technology, Sep. 2007.

[10] B. M. Sathyaraj, L. C. Jain, A. Finn, and S. Drake, "Multiple UAVs path planning algorithms: a comparative study," *Fuzzy Optim Decis Making*, vol. 7, pp. 257–267, 2008.

[11] D. R. Thompson, S. Chien, M. Arrott, A. Balasuriya, Y. Chao, P. Li, M. Meisinger, S. Petillo, and O. Schofield, "Mission Planning in a Dynamic Ocean Sensorweb," in 19^{th} *International Conference on Automated Planning and Scheduling (ICAPS) — Scheduling and Planning Applications woRKshop (SPARK)*, 2009.

[12] D. Kruger, R. Stolkin, A. Blum, and J. Briganti, "Optimal AUV path planning for extended missions in complex, fast-flowing estuarine environments," in *Proceedings of the IEEE International Conference on Robotics and Automation (ICRA)*, 2007.

[13] B. Garau, M. Bonet, A. Alvarez, S. Ruiz, and A. Pascual, "Path Planning for Autonomous Underwater Vehicles in Realistic Oceanic Current Fields: Application to Gliders in the Western Mediterranean Sea," *Journal of Maritime Research*, vol. 6, no. 2, pp. 5–22, 2009.

[14] A. Nash, K. Daniel, S. Koenig, and A. Felner, "Theta*: Any-Angle Path Planning on Grids," in *Proceedings of the AAAI Conference on Artificial Intelligence (AAAI)*, 2007, pp. 1177–1183.

[15] S. Koenig and M. Likhachev, "D* Lite," in *Proceedings of the AAAI Conference of Artificial Intelligence (AAAI)*, 2002, pp. 476–483.

[16] A. Nash, S. Koenig, and M. Likhachev, "Incremental Phi*: Incremental Any-Angle Path Planning on Grids," in *Proceedings of the International Joint Conference on Artificial Intelligence (IJCAI)*, 2009, pp. 1824–1830.

[17] J. G. Graver, "Underwater Gliders: Dynamics, Control and Design," Ph.D. dissertation, Princeton University, may 2005.

[18] N. Mahmoudian and C. Woolsey, "Underwater Glider Motion Control," in *Proceedings of the* 47^{th} *IEEE Conference on Decision and Control*, 2008, pp. 552–557.

[19] B. Garau, A. Álvarez, and G. Oliver, "Path Planning of Autonomous Underwater Vehicles in Current Fields with Complex Spatial Variability: an A* Approach," in *Proceedings of the 2005 IEEE International Conference on Robotics and Automation*, Apr. 2005, pp. 194–198.

[20] E. W. Dijkstra, "A Note on Two Problems in Connexion with Graphs," *Numerische Mathematik*, pp. 269–271, 1959.